

Stripe Formation in Bose-Einstein Condensates with Large Numbers of Vortices

Erich J. Mueller and Tin-Lun Ho

Department of Physics, The Ohio State University, Columbus, Ohio 43210

We analyze recent experiments at JILA which observe periodic formation of stripes in a rotating Bose condensate [Engels et al. Phys. Rev. Lett. **89**, 100403 (2002)], and explain this behavior as a consequence of kinetic energy driven evolution, where the vortices follows a quadrupolar flow. We demonstrate that the structure of vortex lattices in the lowest Landau level is a useful tool for understanding such complex phenomena, even when the system is not in the quantum Hall regime.

PACS numbers: 03.75.Fi

In the last year and a half there have been remarkable developments in producing Bose-Einstein condensates (BEC) with large numbers of vortices[1]. These experiments provide a unique setting for studying the dynamics of vortex lattices. Such experiments would be nearly impossible in a conventional ultra-low temperature laboratory. It is conceivable that even higher angular momentum states can be achieved, eventually producing quantum Hall physics.

The novelty of the dynamics at high angular momentum is demonstrated in a recent experiment at JILA[2]. In this work, after a vortex lattice (with rotation frequency Ω) is created, the stirring force is turned off and a small quadrupolar deformation is suddenly introduced in the trap. The vortex lattice is then rotating against a *static* anisotropic potential. Even for small distortions, the atom cloud undergoes significant ellipsoid deformation. Surprisingly, the vortex lattice transforms periodically into a set of parallel stripes, as if the vortices “melt” into sheets and reappear in a coherent fashion. The stripes appear six times over the rotating period $T = 2\pi/\Omega$, whenever the basis vector of the vortex lattice coincide with the minor axis of the cloud.

There is little question that this intriguing behavior is a general feature of rotating Bose gases with large angular momentum (L), and hence a consequence of the unique physics in this limit. From the view point of energetics, the most significant change as L increases is the rising importance of kinetic energy, which ultimately forces the system into the lowest Landau level. We quantify this consideration by showing that at sufficiently high L , the interactions only perturbatively enter the dynamics, and the time evolution of the vortex lattice is driven by kinetic energy. We calculate analytically the time evolution of the condensate, choosing a variational form of the initial vortex lattice based on its equilibrium structure at even higher angular momentum (i.e. the mean field quantum Hall regime)[3]. Our calculation explains the origin of all the features observed in ref.[2]. The agreements between our results and experimental observations shows that even if the system is not in the quantum Hall regime, the physics of lowest Landau level, which plays an important role in our calculation, is useful for understanding complex phenomena and provides powerful approximation schemes.

I. Kinetic evolution: Justification and evolution of density profile: We are interested the solution of the Gross-Pitaevskii (GP) equation

$$i\hbar\partial_t\Psi(\mathbf{x},t) = (T + V(\mathbf{x}) + g|\Psi(\mathbf{x},t)|^2)\Psi(\mathbf{x},t) \quad (1)$$

with the boundary condition $\Psi(\mathbf{x},t=0) = \Phi(\mathbf{r})$, where $T = -(\hbar^2/2M)\nabla^2$, $\Phi(\mathbf{r})$ is the equilibrium vortex state of a cylindrically potential, $\Psi(\mathbf{r},t)$ is the condensate wavefunction after a quadrupolar distortion is added to the potential at $t=0$, and $V(\mathbf{x})$ is the deformed trap at time $t > 0$. We shall treat the problem as two dimensional, since the effect of the third dimension can be obtained by Thomas-Fermi approximation as in ref.[3]. In this case, we have $V = \frac{1}{2}M(\omega_x^2x^2 + \omega_y^2y^2)$, $\omega_x = \omega(1 + \epsilon)$, $\omega_y = \omega(1 - \epsilon)$, where ϵ is the quadrupolar distortion.

Since $\Phi(\mathbf{r})$ is an equilibrium rotating state, it minimizes the GP functional $\mathcal{F} = \langle h_0 + U - \Omega L_z - \mu N \rangle$, where $h_0 = T + V$, $\langle U \rangle = (g/2) \int |\Phi|^4$, μ is the chemical potential and $L_z = -i\hbar\hat{\mathbf{z}} \cdot \mathbf{x} \times \nabla$. Writing $\Phi(\mathbf{r}) = e^{iS(\mathbf{r})}\sqrt{\rho(\mathbf{r})}$, where S is the phase function and ρ is the density, we have $\mathcal{F} = \int \{ \frac{\hbar^2}{2M} [\nabla\sqrt{\rho}]^2 + \frac{M}{2}(\mathbf{v}_s - \Omega\hat{\mathbf{z}} \times \mathbf{r})^2\rho + [\frac{1}{2}M(\omega^2 - \Omega^2)r^2 - \mu]\rho + \frac{1}{2}g\rho^2 \}$ where $\mathbf{v}_s = (\hbar/M)\nabla S$ is the superfluid velocity. For equilibrium states with large number of vortices, the system has a spatial average $\bar{\mathbf{v}}_s \approx \Omega\hat{\mathbf{z}} \times \mathbf{r}$, and a density is

$$\rho_o \approx (\mu - \frac{1}{2}M(\omega^2 - \Omega^2)r^2)/g. \quad (2)$$

It is important to note that states with large number of vortices can only be achieved when $\Omega \rightarrow \omega$, which means that $\frac{1}{2}M(\omega^2 - \Omega^2)r^2 \ll V(\mathbf{r}) = \frac{1}{2}M\omega^2r^2$. As a result, the $g|\Psi|^2$ term in Eq. (1) can be replaced by a constant ($g|\Psi|^2 \approx \mu$) at early times where $\Psi \approx \Phi$. We show below, however, that this replacement remains valid over the observed period of stripe formation, and the dynamics are governed solely by the kinetic energy, leading us to describe the dynamics as *kinetic evolution*.

Under kinetic evolution, the shape of the condensate is described by the matrix $\mathcal{D}_{ij} = \langle x_i(t)x_j(t) \rangle / [\langle r^2 \rangle / 2]$, where $(x_1, x_2) \equiv (x, y)$, $x_i(t) = e^{i\hbar\omega_x t}x_i e^{-i\hbar\omega_y t}$, and $\langle \dots \rangle$ means average with respect to the initial state Φ . Since $x(t) = c_x x + s_x p_x / (M\omega_x)$, $y(t) = c_y y + s_y p_y / (M\omega_y)$, and $\mathbf{p}\Psi \approx M\Omega\hat{\mathbf{z}} \times \mathbf{r}\Psi$, where $c_x = \cos\omega_x t$, $s_x = \sin\omega_x t$, we have $\langle x_i x_j \rangle = \frac{1}{2}\langle r^2 \rangle \delta_{ij}$, $\langle p_i p_j \rangle = \frac{1}{2}M^2\Omega^2 \langle r^2 \rangle \delta_{ij} \sim$

$\frac{1}{2}M^2\omega^2\langle r^2\rangle\delta_{ij}$, $\langle xp_y\rangle \approx M\Omega\langle x^2\rangle$, and hence

$$\mathcal{D} = \begin{pmatrix} c_x^2 + t_x^2 & c_x t_y - c_y t_x \\ c_x t_y - c_y t_x & c_y^2 + t_y^2 \end{pmatrix} \equiv \begin{pmatrix} \alpha & \gamma \\ \gamma & \beta \end{pmatrix}. \quad (3)$$

where $t_i = s_i\omega/\omega_i$, $i = x, y$. (Eq. (3) can also be derived from the trial wavefunction we use later). Noting that initial density in Eq. (2) is of the form $\rho_o = \bar{\rho}(1 - r^2/\langle r^2\rangle)$, where $g\bar{\rho} = \frac{1}{2}M(\omega^2 - \Omega^2)\langle r^2\rangle$, Eq. (3) implies that with similar approximation, the deformed density is $\rho(\mathbf{r}) = \frac{\bar{\rho}}{\sqrt{\text{Det}\mathcal{D}}}(1 - \mathbf{r} \cdot \mathcal{D}^{-1} \cdot \mathbf{r}/\langle r^2\rangle)$, where the inverse determinant comes from number conservation. The deformed density can be rewritten as

$$\rho(\mathbf{r}) = \frac{\bar{\rho}}{\sqrt{\lambda_+\lambda_-}} - \frac{M(\omega^2 - \Omega^2)}{2g\sqrt{\lambda_+\lambda_-}} \left(\frac{r_+^2}{\lambda_+} + \frac{r_-^2}{\lambda_-} \right) \quad (4)$$

where λ_{\pm} and $\hat{\mathbf{n}}_{\pm}$ are the eigenvalues and eigenvectors of \mathcal{D} , ($\lambda_+ > \lambda_-$, $\hat{\mathbf{n}}_+ \cdot \hat{\mathbf{n}}_- = 0$), and $r_{\pm} = \mathbf{r} \cdot \hat{\mathbf{n}}_{\pm}$. To be able to replace $g\rho$ in Eq. (1) by a constant, one needs $g\rho \ll \frac{1}{2}M\omega^2(r_+^2 + r_-^2)$, or

$$1 - \Omega/\omega \ll \lambda_- \sqrt{\lambda_+\lambda_-}. \quad (5)$$

In Fig. 1a, we plot the λ -product in Eq. (5) and the aspect ratio $\sqrt{\lambda_-/\lambda_+}$ of the ellipsoidal density profile Eq. (4) as a function of ωt for $\epsilon = 0.036$. It is clear that Eq. (5) remains valid up to 2.5 to 3 times of the original period $2\pi/\omega$ for rotating states with $1 - \Omega/\omega \sim 10^{-2}$. One can see from fig.1a that even for $\epsilon = 0.036$, the aspect ratio reaches 50% when $\omega t \approx 3\pi$ [5]. In fig.1b, we have plotted the orientation of the minor axis $\hat{\mathbf{n}}_- \equiv (\cos\chi, \sin\chi)$, where χ can be found from Eq. (3) to satisfy $\tan 2\chi = \gamma/(\alpha - \beta)$. We see that $\hat{\mathbf{n}}_-$ starts at $\hat{\mathbf{x}}$, and then rotate by 45° in half a period and stays around that value for some time. Eventually it will rotate back to $\chi \approx 0$, but only at times much longer than that for which kinetic evolution is valid.

For the rest of the paper we shall stay within the time interval where kinetic evolution is valid. Eq. (1) then gives

$$\Psi(\mathbf{x}, t) = \int G(\mathbf{x}, \mathbf{x}'; t) \Phi(\mathbf{x}') d\mathbf{x}', \quad (6)$$

where $G(\mathbf{x}, \mathbf{x}'; t) = \langle \mathbf{x} | e^{-i\hbar\omega t/\hbar} | \mathbf{x}' \rangle$, $h_0 = \mathbf{p}^2/2M + M(\omega_x^2 x^2 + \omega_y^2 y^2)/2$, which can be shown to be

$$G(\mathbf{r}, \mathbf{r}'; t) = \mathcal{A}e^{(i/2)(\mathbf{r} \cdot \mathcal{Q} \cdot \mathbf{r} + \mathbf{r}' \cdot \mathcal{Q} \cdot \mathbf{r}' - 2\mathbf{r} \cdot \mathcal{P} \cdot \mathbf{r}')}, \quad (7)$$

$$\mathcal{Q} = \frac{1}{a^2} \begin{pmatrix} c_x/t_x & 0 \\ 0 & c_y/t_y \end{pmatrix}, \quad \mathcal{P} = \frac{1}{a^2} \begin{pmatrix} 1/t_x & 0 \\ 0 & 1/t_y \end{pmatrix} \quad (8)$$

and $\mathcal{A} = (2\pi a^2)^{-1} \sqrt{\frac{c_x c_y}{-t_x t_y}}$, where $a^2 = \hbar/(M\omega)$.

II. The evolving condensate: For later discussions, we represent the basis vector $\mathbf{b}_1, \mathbf{b}_2$ of a vortex lattice as complex numbers $b_i = \mathbf{b}_i \cdot (\hat{\mathbf{x}} + i\hat{\mathbf{y}})$, $i = 1, 2$, and define $\tau \equiv b_2/b_1 = u + iv$, where u and v are the real and imaginary part of τ . The entire lattice will be denoted

as $\{b\}$, where $b = \ell_1 b_1 + \ell_2 b_2$, and ℓ_1, ℓ_2 are integers; and the size of unit cell is $|b_1|^2 |v|$. The choice of basis is not unique. A natural choice is the ‘‘fundamental set’’ (\bar{b}_1, \bar{b}_2) containing the two shortest non-parallel vectors in the lattice. As well known from Conformal Analysis, this set is confined in the ‘‘fundamental’’ region ($|\tau| > 1, |u| < 1/2, v > 0$), and that for any basis (b_1, b_2) one can find an *image* (\bar{b}_1, \bar{b}_2) in the fundamental region by basis transformation. Because the way the basis vectors are chosen, the fundamental region is best for describing the stretching of lattices. To distinguish the initial hexagonal lattice from others at later time, we label its quantities with a superscript ‘‘o’’. Thus, $\tau^o = e^{i\pi/3}$, $|b_1^o| = |b_2^o|$.

To allow for an analytic calculation of the condensate dynamics we use a variational form of the initial state,

$$\tilde{\Phi}(\mathbf{r}) = C \prod_{b^o} (z - b^o) e^{-r^2/(2d^2)} \quad (9)$$

where $z = x + iy$, C is a normalization constant, The lengths d and $|b_1^o|$ are variational parameters obtained by minimizing the energy $h_0 + U - \Omega L_z - \mu N$. Eq. (9) is the form that will emerge in the mean field quantum Hall regime[3], (in which case d is no longer be a variational parameter but is equal to the trap length a exactly). The minimization process is similar to the one described in ref.[3]. Since our results do not depend on the numerical value of the optimal parameters but only their *general features*, we shall only list the relevant features and not dwell on the details of the minimization process. These features include:

- (a) A condensate with large number of vortices has rotational frequency $\Omega \rightarrow \omega$, and $d \rightarrow a$.
- (b) The vortices form a triangular lattice with averaged vorticity $(2\pi\hbar/M)/v_c^o = 2\Omega \approx 2\omega$, which gives $v_c^o = \pi a^2$, and $|b_1^o|^2 = |b_2^o|^2 = 2\pi a^2/\sqrt{3}$.
- (c) The overall density of $\tilde{\Phi}(\mathbf{r})$ Gaussian with a width σ ($\sigma^2 = \langle r^2 \rangle_{\tilde{\Phi}}$) such that $\sigma^{-2} = d^{-2} - \pi v_c^{-1}$. Since $d \approx a$, we have $\sigma \gg a$.
- (d) $\tilde{\Phi}$ satisfies the lowest Landau level constraint $[(p_x + ip_y) + \hbar z/d^2]\tilde{\Phi} = 0$. It is straightforward to show from this condition that \mathcal{D} is given by Eq. (3) when $\sigma^2 \gg d^2$.
- (e) Apart from a proportionality constant, $\tilde{\Phi}(\mathbf{r})$ is the Weierstrass σ -function[6].

To proceed with the integration in Eq. (6), we use the relation between the Weierstrass σ -function and the θ -function to write $\tilde{\Phi}$ as [4, 6]

$$\tilde{\Phi}(\mathbf{r}) = \theta(\mathbf{q}_o \cdot \mathbf{r}, \tau_o) e^{\pi(x+iy)^2/(2v_c^o)} e^{-r^2/(2d^2)} \quad (10)$$

where $\mathbf{q}_o = (\hat{\mathbf{x}} + i\hat{\mathbf{y}})/b_1^o$, $\tau_o = e^{2\pi i/3}$, and

$$\theta(\zeta, \tau) \equiv \frac{1}{i} \sum_{n=-\infty}^{\infty} (-1)^n e^{i\pi n(n+1/2)\tau} e^{2\pi i\zeta(n+1/2)}. \quad (11)$$

We have set the normalization constant in Eq. (10) to 1 because it is not important for our discussions. To

proceed further, we rewrite $\tilde{\Phi}$ as

$$\begin{aligned}\tilde{\Phi}(\mathbf{r}) &= \theta(\mathbf{q}_o \cdot \mathbf{r}, \tau_o) e^{-\frac{1}{2}\mathbf{x} \cdot \mathcal{M}_o \cdot \mathbf{x}}, \\ \mathcal{M}_o &= \begin{pmatrix} \frac{1}{d^2} - \frac{\pi}{v_c^2} & -i\frac{\pi}{v_c^2} \\ -i\frac{\pi}{v_c^2} & \frac{1}{d^2} + \frac{\pi}{v_c^2} \end{pmatrix} \approx \frac{1}{d^2} \begin{pmatrix} 0 & -i \\ -i & 2 \end{pmatrix}\end{aligned}\quad (12)$$

The approximate form is due to properties (a) and (c) mentioned above.

Because of the Gaussian structure in Eqs. (11), (12), and (7), the integral (6) is also a Gaussian. After sorting out terms containing $(n + 1/2)^2$ and $(n + 1/2)$ in the exponent, $\Psi(\mathbf{r}, t)$ can be recast into a form similar to Eq. (10),

$$\Psi(\mathbf{r}, t) = \mathcal{B}\theta(\mathbf{q} \cdot \mathbf{r}, \tau) e^{-\frac{1}{2}\mathbf{x} \cdot \mathcal{M} \cdot \mathbf{x}} \quad (14)$$

$$\mathcal{M} = \mathcal{P}\Lambda^{-1}\mathcal{P} - i\mathcal{Q}, \quad \Lambda = \mathcal{M}_o + i\mathcal{Q}, \quad (15)$$

$$\mathbf{q} = -i\mathcal{P}\Lambda^{-1}\mathbf{q}_o, \quad \mathbf{q}_o = (\hat{\mathbf{x}} + i\hat{\mathbf{y}})/b_1^o, \quad (16)$$

$$\tau = \tau_o + \eta, \quad \eta = i2\pi\mathbf{q}_o \cdot \Lambda^{-1} \cdot \mathbf{q}_o \quad (17)$$

$$\mathcal{B} = 2\pi\mathcal{A}/\sqrt{|\text{Det}[\Lambda]|}. \quad (18)$$

Equations (14) to (18) are the key results of this paper. An important feature of Eq. (14) is that the zeros (i.e. the vortices) of $\Psi(\mathbf{r})$ continue to organize in a lattice during the evolution, with basis vectors (\mathbf{b}_1 and \mathbf{b}_2) given by

$$\mathbf{q} \cdot \mathbf{b}_1 = 1, \quad \mathbf{q} \cdot \mathbf{b}_2 = \tau, \quad (19)$$

as a consequence of the quasiperiodicity properties, $\theta(\zeta + 1, \tau) = -\theta(\zeta, \tau)$, and $\theta(\zeta + \tau, \tau) = -\theta(\zeta, \tau)e^{-i\pi(\tau+2\zeta)}$. One can see from Eq. (14) that the vortices follow a velocity field $V(\mathbf{x}) = Q_{ij}x_j$, where $Q_{ij}(t) = [(\partial_i \mathbf{b}_{1j})\mathbf{K}_{1j} + (\partial_i \mathbf{b}_{2j})\mathbf{K}_{2j}]/(2\pi)$, and \mathbf{K}_i 's are the reciprocal basis vectors, $\mathbf{K}_i \cdot \mathbf{b}_j = 2\pi\delta_{i,j}$. The symmetric and antisymmetric part of Q_{ij} correspond to a quadrupolar and a rotational flow. Thus, apart from an overall rotation, the vortices follow the streamlines of a quadrupolar flow.

By properties (a) and (b), the parameters of Eq. (14), are approximately $d \approx a$, $|b_1^o|^2 \approx 2\pi a^2/\sqrt{3}$, which fully specifies \mathbf{q} , τ , \mathcal{M} and \mathcal{D} [7]. While our results hold for arbitrary ϵ , we shall focus on small deformations $\epsilon \ll 1$ in order to compare with current experiments[2]. In Fig. 2, we have plotted the density of the system at 8 equal time intervals between $\omega t = 0$ and 6 for $\epsilon = 0.036$ and $\Omega = 0.92\omega$. Stripes appear periodically, becoming more distinct at each subsequent appearance.

To illustrate the relation between lattice deformation and stripe formation, we find the images (\bar{b}_1, \bar{b}_2) of basis vectors obtained from Eq. (19) in the fundamental region. The stretching of the lattice is then describe by the ratio $\bar{\tau} = \bar{b}_1/\bar{b}_2 = \bar{u} + i\bar{v}$. Large stretching is given by large $|\bar{\tau}|$ or by large \bar{v} since $|\bar{u}| < 1/2$. In Fig. 3, we have plotted \bar{v} and the angle ϕ between \bar{b}_1 and x axis as a function of ωt at the lower panel. We find that (i) stripes are most pronounced when \bar{v} is a maximum, which occurs six times within a period ωt . Moreover, the sharpness of stripe density increases with time; (ii) the maximum

occurs when ϕ is 45° , which is the direction of the minor axis after half of the period as shown in Fig. 1b. These two detailed features are in exact agreement with those observed in ref.[2]. The discontinuities in ϕ are due to the mapping of the basis vectors back into the fundamental region when the lattice is stretched. The orientation of the second basis vector \bar{b}_2 is given in the top panel of fig.3, where we plot the relative angle κ between \bar{b}_1 and \bar{b}_2 . Once again, the discontinuities of this angle is due to the mapping back to the fundamental region. To illustrate the *continuous* evolution of the lattice and the discontinuous change of the fundamental basis, we have plotted the lattices and indicated their fundamental basis at different times in Fig. 4. It is also interesting to note that at the cusps in fig. 3, the unit cell of vortex lattice is close to a square.

(III) The origin of stripe formation: Figure 3 and 4 show that vortex stripes can be produced by rather moderate changes in the basis vectors. This sensitivity is due to the special coherent properties of the vortex lattice, as revealed by studying the periodic part of the density which is calculated from [4],

$$|\theta(\zeta, \tau)|^2 = \left[\frac{1}{v_c} \sum_{\mathbf{K}} g_{\mathbf{K}} e^{i\mathbf{K} \cdot \mathbf{r}} \right] e^{2\pi y^2/v_c} \quad (20)$$

where $\mathbf{K} = m_1\mathbf{K}_1 + m_2\mathbf{K}_2$ are the reciprocal lattice vectors, m_i are integers, and $g_{\mathbf{K}} = (-1)^{m_1+m_2+m_1m_2} e^{-v_c|\mathbf{K}|^2/8\pi} \sqrt{v_c/2}$. Because of the rapid decay of $g_{\mathbf{K}}$ with increasing $|\mathbf{K}|$, only a few \mathbf{K} vectors around the origin have non-trivial contribution to the density. For a triangular lattice, it is natural to organize the \mathbf{K} - *points* into concentric hexagonal rings, corresponding to reciprocal lattice vectors of roughly equal length, and to number these rings, starting from the origin. The same labeling works for distorted lattices, and for sufficiently small distortions the first ring, made up of the six shortest wavevectors, has the largest contribution to the density. As $|\tau| = |b_2/b_1|$ increases, b_1 becomes the shortest vector in real space, which in turn makes $\pm\mathbf{K}_1$ the shortest vector in k-space, and this wave-vector dominates the contribution from the first ring. Similarly, $\pm 2\mathbf{K}_1$ dominates the contribution from the second ring, and so on. As a result, the density is increasingly dominated by the sum of $g_{\mathbf{K}}$'s containing only integer multiples of \mathbf{K}_1 , which gives rise to a sequence of stripes in real space.

Final Remarks: We have shown that the mysterious periodic stripe formation in ref.[2] reflects the kinetic evolution of the vortex lattice, where vortices remained organized in lattice, with each vortex following the streamline of a quadrupolar flow. The six occurrences of stripes during a period is caused by an almost periodic deformation of the vortex lattice and not the melting of vortices into sheets. The method presented here should also be applicable to other to dynamical phenomena at high angular momenta and to more complex condensates [8].

This work is supported by NASA Grants NAG8-1441, NAG8-1765, and by NSF Grants DMR-0109255, DMR-

0071630.

- [1] K. W. Madison, et.al, Phys. Rev. Lett. **84**, 806 (2000). J. R. Abo-Shaeer, et.al Science, **292**, 476 (2001). P.C. Haljan, et.al, Phys. Rev. Lett. **87**, 210403 (2001).
- [2] P. Engels, I. Coddington, P. C. Haljan, and E. A. Cornell Phys. Rev. Lett. **89**, 100403 (2002).
- [3] Tin-Lun Ho, Phys. Rev. Lett. **87**, 060403 (2001).
- [4] Erich J. Mueller and Tin-Lun Ho Phys. Rev. Lett. **88**, 180403 (2002).
- [5] The large response is due to the fact that one is near the resonance of the $m = -2$ mode.
- [6] See p.52 and 60 of K. Chandrasekharan, *Elliptic Functions* (Springer-Verlag, New-York, 1985).
- [7] As an illustration, for times $2\epsilon\omega t \ll 1$, which include $\omega t > 1$, we have $\eta = \epsilon\sqrt{3}e^{-2i\omega t}(-2\omega t + \sin 2\omega t) + O(\epsilon^2)$ from Eq. (17), and $\mathbf{q} = \nu(t)(\hat{\mathbf{x}} + i\hat{\mathbf{y}})/b_1^0 + \xi(t)(\hat{\mathbf{x}} - i\hat{\mathbf{y}})/b_1^0$ from Eq. (16), with $\xi = -i\epsilon e^{-2i\omega t} [e^{i\omega t}\omega t - \sin(\omega t)]$, and $\nu = e^{-3i\omega t} [e^{2i\omega t} + i\epsilon(2\omega t - \sin(2\omega t))]$. If we define $q_{\pm} = \mathbf{q} \cdot (\hat{\mathbf{x}} \pm i\hat{\mathbf{y}})$, then $q_+ = 2\xi/b_1^0$, $q_- = 2\nu/b_1^0$, and Eq. (19) implies $b_1q_- + b_1^*q_+ = 2$. We then have $b_1/b_1^0 = e^{i\omega t} - i\epsilon[e^{-i\omega t}\omega t - \sin(\omega t)] + O(\epsilon^2)$. All our calculations, however, are performed with the exact expressions Eq. (15) to (18) without expansions.
- [8] Professor Crispin Gardiner recently informed us that he has also found stripes in a numerical simulation of a modified GP equation which includes dissipation.

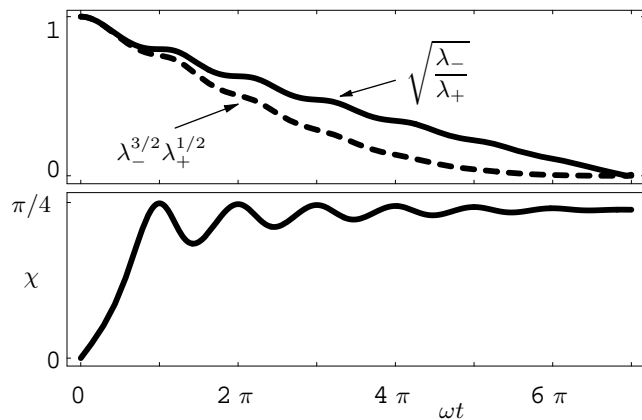


FIG. 1: (a) The product $\lambda_-^{3/2}\lambda_+^{1/2}$ and the aspect ratio $\sqrt{\lambda_-/\lambda_+}$ for $\epsilon = 0.036$. (b) The angle χ between the minor axis $\hat{\mathbf{n}}_-$ and the x -axis.

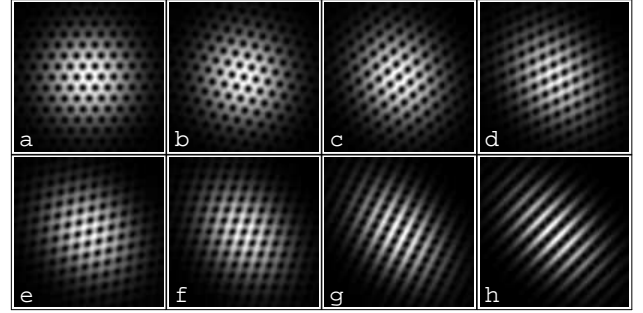


FIG. 2: Density profile of the evolving condensate from $\omega t = 0$ to 6 at equal time interval. Dark color means low density. Panel (h) corresponds to point (c) on Fig. 3.

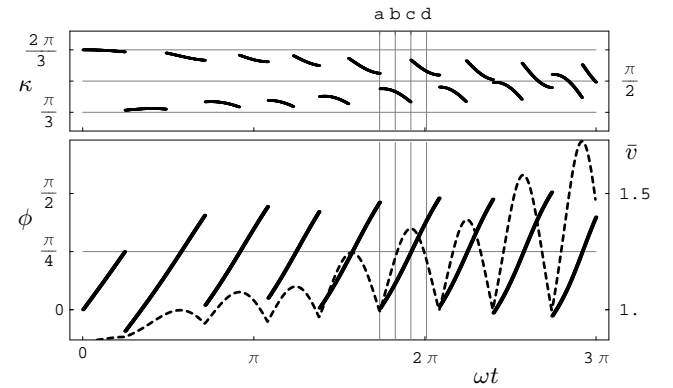


FIG. 3: The lower panel shows \bar{v} (dotted line) and the angle ϕ between $\bar{\mathbf{b}}_1$ and the x -axis as a function of ωt . The peaks of \bar{v} correspond to the appearance of stripes, and coincide with $\phi = \pi/4$; i.e. $\bar{\mathbf{b}}_1$ aligned with the minor axis. The upper panel shows the angle κ between the vectors $\bar{\mathbf{b}}_2$ and $\bar{\mathbf{b}}_1$. The lattice configuration and basis vectors at times (a), (b), (c), (d) are shown in Fig. 4.

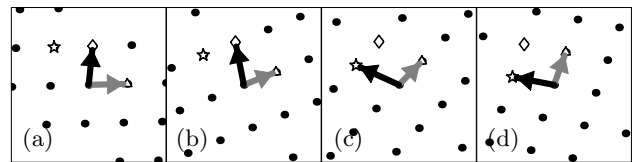


FIG. 4: The lattice configurations and the basis vectors in the fundamental region at different time (a), (b), (c), (d) indicated in Fig. 3. The discrete change of basis vectors between (b) and (c) is due to the mapping back to the fundamental region.